Highly Stable Anion Exchange Membranes with Internal Cross-Linking Networks

Wanxing Xu, Yuyue Zhao, Zhizhang Yuan, Xianfeng Li, Huamin Zhang,* and Ivo F. J. Vankelecom*

Anion exchange membranes (AEMs) with excellent stability and high ion conductivity are fabricated via the formation of internal cross linking networks. The internal crosslinking networks are constructed by reacting 4,4′-bipyridine with chloromethylated polysulfone. The bipyridine group simultaneously functions as ionic conductor and cross linker in this system. The performance of the membrane is tuned via controlling the 4,4′-bipyridine content in the casting solution. The prepared membranes demonstrate excellent chemical stability and high ion conductivity under acidic conditions. As a consequence, the membranes show very promising performance for vanadium flow battery application, exhibiting a Coulombic efficiency of 99.2% and an energy efficiency of 81.8% at a current density of 140 mA cm^{-2}. The battery that is assembled with the prepared membrane shows a stable battery performance over more than 1600 cycles, which is by far the longest cycle life reported. These results indicate that the AEMs with internal crosslinking structures are promising candidates for battery systems and even for fuel cells.

1. Introduction

Anion exchange membranes (AEMs) have attracted wide attention in both battery systems and alkaline fuel cells, where they isolate active species, while still allowing transport of ions to complete the electrical circuit.[1] Such membranes can be based on a variety of polymers, possibly transformed into composite materials containing fillers. For example, a variety of AEMs based on PSFs, polyphenylenes, polystyrenes, polyethylenes, poly(arylene ether ketone)s, and poly(phenylene oxide)s have been well studied in the application of flow batteries and fuel cells.[2] However, one of the major concerns of AEMs is their low chemical stability under battery operating conditions.[1,3] It has been shown that the quaternary ammonium groups, which are the mostly studied anion exchange groups, undergo several degradation pathways in alkaline environments at elevated temperatures.[4] In an acidic and oxidizing battery system, the stability of AEMs needs to be further improved as well. Therefore, the development of AEMs with high chemical stability is one of the most important and challenging topics.[5] Much efforts have been dedicated to fabricate such AEMs. It has been proven that cross linking can significantly improve the hydrolytic and oxidative stability of the membranes.[2c,6] Hence, a better chemical stability could be achieved for membranes with well-connected network structures through the cross linking.[7] For example, Zhang et al. fabricated a composite AEM based on polysulfone (PSF) and polyvinylidene difluoride (PVDF) via a dication cross-linking strategy for the application of vanadium flow battery (VFB). The VFB assembled with this kind of AEM exhibited a columbic efficiency (CE) of 99% and an energy efficiency (EE) of 84% at a current density of 80 mA cm^{-2}, while it kept a stable performance after running for more than 900 cycles.[6] Miyake et al. investigated the effect of ammonium groups (trimethylamine, *N*-butyldimethylamine, 1-methylimidazole, 1,2-dimethylimidazole, and pyridine) on the stability of AEMs in alkaline medium, proving that AEMs with pyridine groups showed good alkaline and hydrazine stability due to the high basicity of pyridine and the delocalized cations in conjugated pyridinium rings.[8]

In this paper, an AEM is presented consisting of internal crosslinking networks (In-AEM) based on PSF. 4,4′-Bipyridine was selected as both ammonium source and cross-linking agent due to the two amine groups in the bipyridine ring and its symmetrical structure, while chloromethylated polysulfone (CMPSF) was selected as matrix. The bipyridine connects with the CMPSF to establish the internal cross linking structure and provide ion conductivity (**Scheme 1**). These crosslinked membranes are expected to combine high ion selectivity and high ion conductivity with excellent chemical stability. The structure and physicochemical properties were characterized in detail. The performance and stability of the prepared membranes were verified by applying them in a VFB, which is considered to be a promising alternative to existing large-scale energy

W. Xu, Y. Zhao, Z. Yuan, Prof. X. Li, H. Zhang
Division of Energy Storage
Dalian Institute of Chemical Physics
Chinese Academy of Sciences
Zhongshan Road 457, Dalian 116023, China
E-mail: lixianfeng@dicp.ac.cn; zhanghm@dicp.ac.cn
W. Xu, Y. Zhao, Z. Yuan
University of Chinese Academy of Sciences
Beijing 100039, China
Prof. I. F. J. Vankelecom
Centre for Surface Chemistry and Catalysis
Faculty of Bioscience Engineering
Katholieke Universiteit Leuven (KU Leuven)
Kasteelpark Arenberg 23 – Box 2461, B-3001 Leuven, Belgium

DOI: 10.1002/adfm.201500284

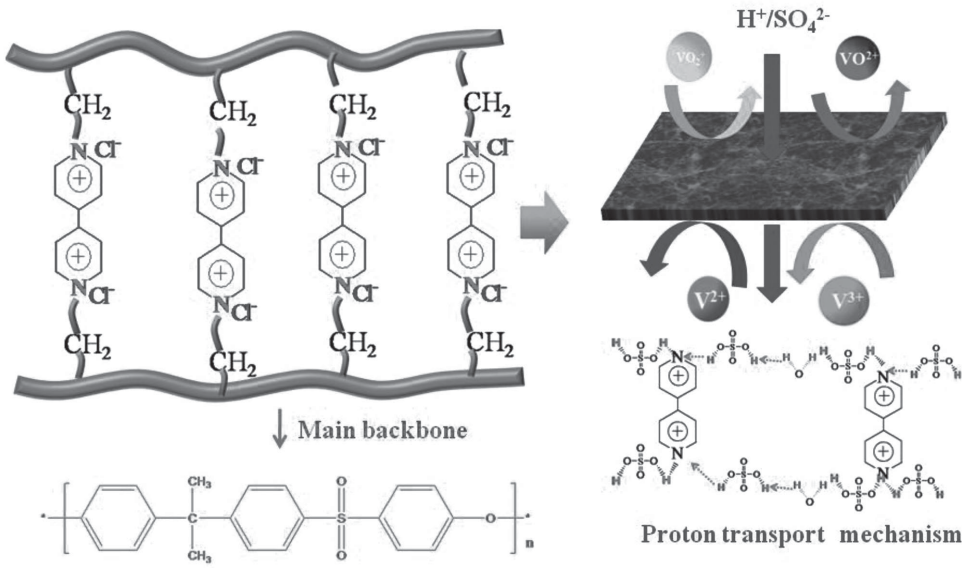

Scheme 1. Schematic principle of membranes with internal crosslinking networks.

storage techniques due to advantages of high efficiency, good operational reliability and long cycle life. In a VFB, a membrane is responsible for separating the positive and negative electrolyte and transferring ions from anode to cathode or vice versa.[1] Thus, an ideal membrane for VFB should possess low permeability of vanadium ions, high ion conductivity and excellent long-term chemical stability.[3,9] Among various types of membranes, AEMs have received extensive attention due to the Donnan exclusion effect by fixed cationic groups to minimize the cross-mixing of vanadium ions.[10] However, AEMs are still limited by their low stability.[4a,11] The prepared AEMs in this paper are expected to perfectly solve this problem and provide more options for VFB membrane development.

2. Results and Discussion

In the present paper, In-AEMs were fabricated by reacting CMPSF with 4,4′-bipyridine. The cross linking degree and the content of anion conductive pyridine groups were tuned via changing the content of 4,4′-bipyridine. The membranes prepared from different content of bipyridine were referred to as CMPSF-*X*, where *X* is the ratio of 4,4′-bipyridine to chloromethyl groups of CMPSF. The prepared membranes are schematically represented in Scheme 1.

The Fourier transform IR (FTIR) spectra of plain CMPSF and In-AEMs prepared from different bipyridine concentrations are displayed in **Figure 1**. The absorption band at 755 cm^{-1} in the spectrum of the parent CMPSF membrane is attributed to the characteristic absorption of the C–Cl in CMPSF, confirming the successful introduction of chloromethyl groups in PSF. Compare with this parent CMPSF, a new absorption at around 1520 cm^{-1}, attributed to the stretching of the pyridine C=N bond, was clearly observed in all prepared membranes, indicating the successful introduction of pyridine groups in the prepared membranes.[12] Meanwhile, the band at 755 cm^{-1} disappeared after introducing pyridine in CMPSF, suggesting that the chloromethyl groups reacted almost completely with 4,4′-bipyridine.

Transmission electron microscope (TEM) analysis was carried out on CMPSF-0.7 and CMPSF-0.9 after $[PdCl_4]^{2-}$-staining to investigate the distribution of the positively charged ammonium groups in the prepared membranes. As shown in **Figure 2**, the dark regions were attributed to the clusters formed via the interaction between $[PdCl_4]^{2-}$ and the positively charged pyridine groups,[13] showing the uniform distribution of hydrophilic domains formed via ammonium groups in the cross-section of the In-AEMs. With increasing bipyridine content, the hydrophilic domains become more connected, which is crucial to improve the ion conductivity of the membranes.

Water uptake, swelling, and ion exchange capacity (IEC) data of the prepared membranes are shown in **Table 1**. The IEC of the membranes increases from 1.30 to 1.76 meq g^{-1} with increasing bypridine content, while water uptake and swelling

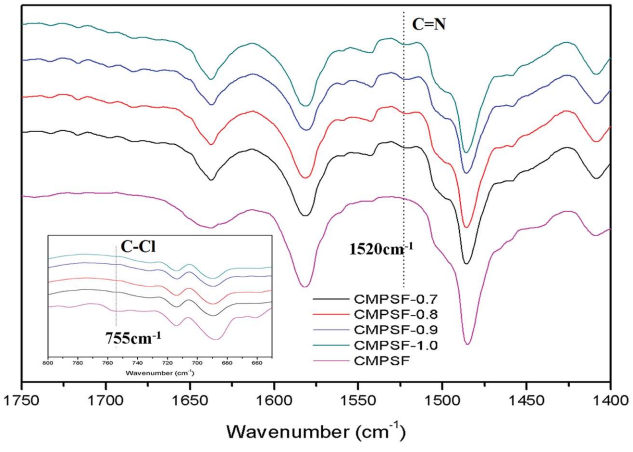

Figure 1. FTIR of CMPSF based membranes.

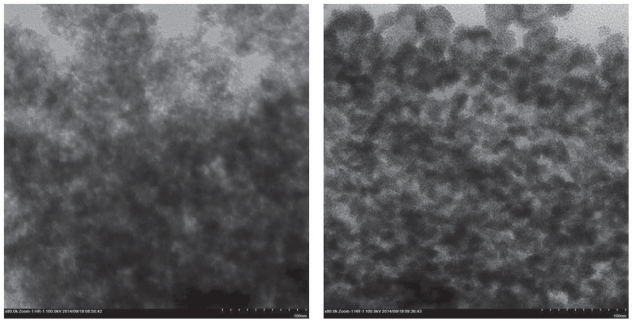

Figure 2. TEM of CMPSF membranes (Left: CMPSF-0.7, Right: CMPSF-0.9).

of the prepared membranes did not change significantly with increasing bipyridine content. This is possibly due to the combined effects from cross linking and increased hydrophilicity. With higher content of hydrophilic bipyridine groups, more water is expected to be absorbed, while the increased cross linking degree derived from high content of biyridine groups will suppress the swelling.[14]

Figure 3 shows the vanadium permeability of Nafion 115 and the In-AEM membranes. The slope of the line corresponding to Nafion 115 is much higher than that of the In-AEM membranes, indicating that vanadium ions transport through the In-AEM membrane at a much lower rate than through Nafion 115. This result is mainly due to two factors: (1) owing to the Donnan exclusion effect, the existence of positively charged pyridine groups restricts the vanadium permeation across the membrane and (2) the well-connected cross linking networks greatly restrict the vanadium ions permeation as well. With increasing bipyridine content, the permeation of vanadium ions hardly changes, in line with the water uptake tendency. Thus, the combined effect of cross linking and the hydrophilic nature of the pyridine groups lead to membranes with high selectivity and high ion conductivity.

The ion conductivity of In-AEM membranes is shown in **Figure 4**. As the 4,4′-bipyridine content increasing, the ionic conductivity increases from 0.15 to 0.26 S cm^{-1} due to the increased content of bipyridine groups and hence of the IEC. Moreover, as displayed in **Figure 5**, the area resistance of In-AEM membrane decreased from 0.81 to 0.13 Ω cm^2 with the 4,4′-bipyridine content increasing from 0.7 to 1.0, which is well in accordance with the results of ion conductivity.

Combining the analyses above, In-AEMs with internal crosslinking network structure exhibit excellent ion selectivity and high ion conductivity, which open prospects for

Table 1. Characteristics of prepared membranes.

Code	Chloromethyl group [$\times 10^{-3}$ M]	Bipyridine [$\times 10^{-3}$ M]	IEC [$\times 10^{-3}$ M g^{-1}]	Water uptake [%]	Swelling [%]
CMPSF-0.7	1	0.7	1.30	11.88	5.46
CMPSF-0.8	1	0.8	1.39	12.77	5.45
CMPSF-0.9	1	0.9	1.54	11.86	4.74
CMPSF-1.0	1	1	1.76	11.78	5.58

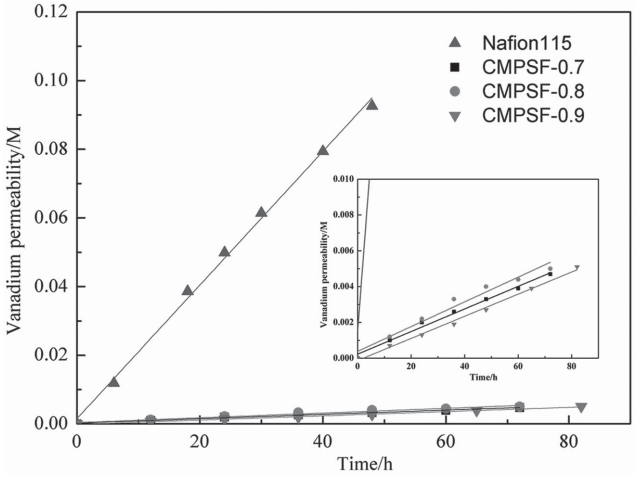

Figure 3. VO^{2+} concentration versus time at the deficiency side of the diffusion cell with Nafion 115 and In-AEM membranes.

outstanding VFB performance. First, the VFBs assembled with In-AEMs with different 4,4′-bipyridine content were tested at a current density of 80 mA cm^{-2}, as reported in **Figure 6**. The CE, which is determined by the ratio of a cell's discharge capacity to its charge capacity, remained above 98%, indicating the excellent ion selectivity of all prepared In-AEMs. The voltage efficiency (VE), defined as the ratio of a cell's mean discharge voltage divided by its mean charge voltage, increased from 85.8% to 88.5% along with the 4,4′-bipyridine content, which agrees well with the ion conductivity results. The EE, an important parameter to evaluate an energy storage system increases strongly from 84.4% to 87.1% with increasing 4,4′-bipyridine content.

Figure 7 shows the performance of a VFB single cell assembled with CMPSF-0.9 under different current densities. The CE increases from 98.5% to 99.2% along with the current density ranging from 80 to 140 mA cm^{-2}. This is because a charge/discharge cycle is finished within less time at a higher current density. However, the VE decreases from 89.6% to 82.5% with increasing the current density from 80 to 140 mA cm^{-2}. This result is mainly attributed to the higher overpotential and

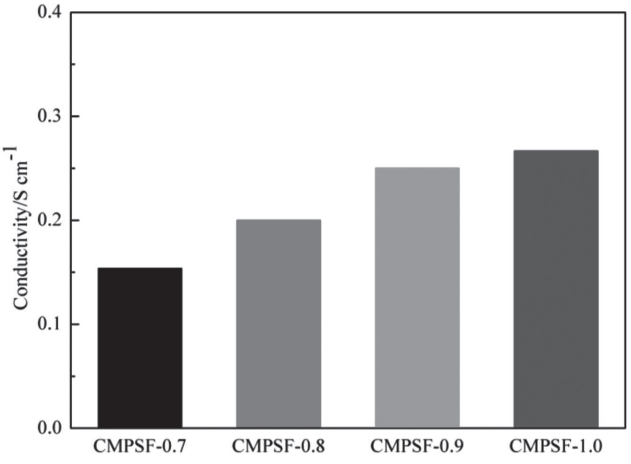

Figure 4. Ion conductivity of In-AEM membranes.

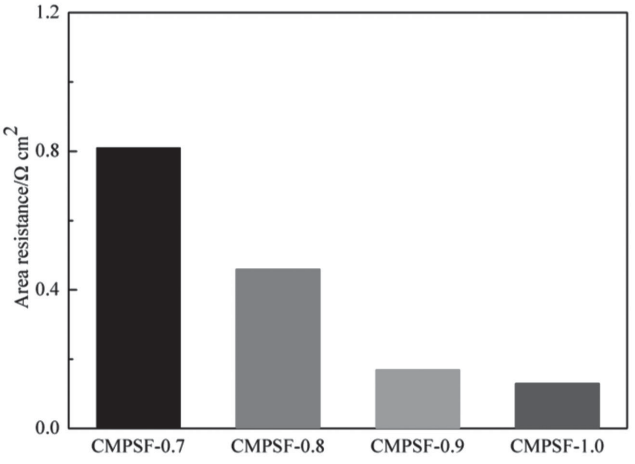

Figure 5. Area resistance of In-AEM membranes.

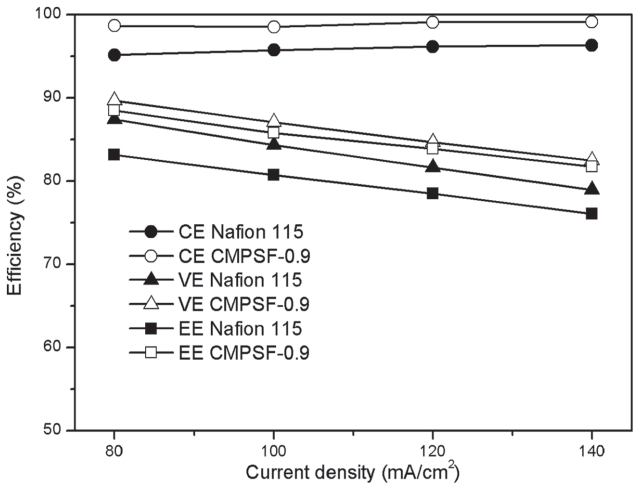

Figure 7. VFB performance of membrane CMPSF-0.9 and Nafion 115 under different current densities.

ohmic resistance at a higher current density. As a consequence, this membrane exhibits a CE of 99.2% and EE of 81.8% at a current density of 140 mA cm^{-2}, which is by far one of the most promising results ever obtained. Compared with commercial Nafion 115 (CE = 96.5%, EE = 76.1%), the prepared membrane shows an overall much higher performance at a current density of 140 mA cm^{-2}, indicating that the In-AEMs with well-connected cross linking structures could serve as promising separators for VFBs.

To investigate the chemical stability of the In-AEM under strong acidic conditions, a VFB assembled with CMPSF-0.9 was cycled at a current density of 140 mA cm^{-2}. As illustrated in **Figure 8**, no obvious efficiency decline can be observed after running for more than 1600 cycles. The cycle life is by far the longest ever reported, demonstrating the excellent stability of the prepared membrane under VFB operating medium. The membrane morphology after this cycle life test was investigated by scanning electron microscope (SEM) (See Supporting Information Figure S1). No obvious defects were detected on the membrane cross section or surface, further confirming the high stability of prepared membranes.

To further verify the membrane stability, an accelerating oxidizing experiment was carried out on CMPSF-0.9 by immersing it in 1.5 M (V) for 3 days at 40 °C. Under such conditions, Sulfonated poly (ether sulfone) (SPES) or SPEEK membranes would readily break into pieces.[15] Afterward, the VFB single cell test was performed on the treated membrane. The VFBs assembled with this treated membrane showed a CE of 98%, and an EE of 81% at a current density of 140 mA cm^{-2}, which is similar with the untreated membranes. These results thus further confirmed the excellent stability of prepared In-AEM membranes (**Figure 9**).

2.1. The Transfer Behavior and Capacity Retention of In-AEMs

The loss of capacity over cycling is a significant issue with AEMs for VFBs.[16] **Figure 10** shows the molar quantity of total vanadium ion at the positive and negative side, when employing

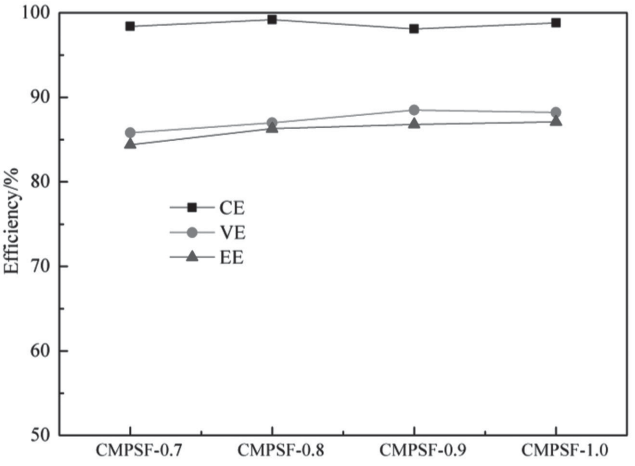

Figure 6. VFB performance of In-AEM fabricated with different 4,4′-bipyridine content.

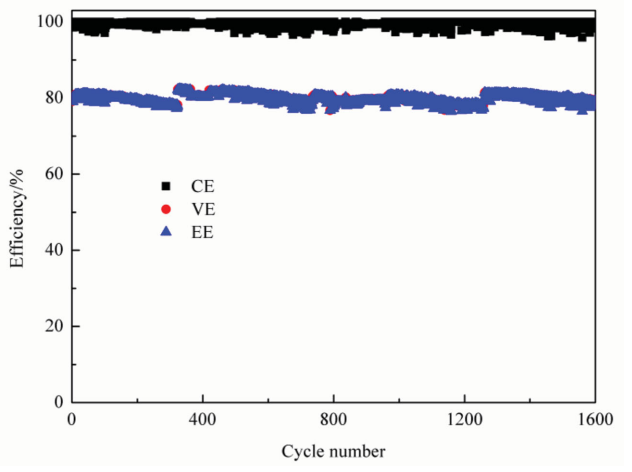

Figure 8. Cycling performance of VFB assembled with membrane CMPSF-0.9 at a current density of 140 mA cm^{-2}.

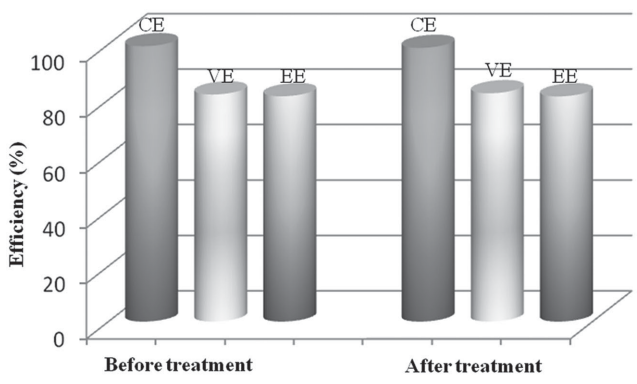

Figure 9. The performance of CMPSF-0.9 before and after accelerating oxidizing test.

CMPSF-0.9 and Nafion 115 as a membrane during the cycling test. For CMPSF-0.9, as the cycle proceeds, the molar quantity of vanadium ions slowly decreased on the positive side and increased on the negative side, suggesting that vanadium ions transfer from the positive to the negative half-cell. This imbalance between the positive and negative half-cell will render the positive electrolyte the "limiting electrolyte." That is, the molar quantity of vanadium active species in the positive half-cell is lower than that in the negative half-cell. On the contrary, the molar quantity of vanadium ions slowly increased on the positive side and decrease on the negative side, when employing Nafion 115 as membrane. Compare with Nafion 115, the prepared CMPSF-0.9 shows much slower transfer rate of vanadium ions, further leading to much less imbalance. The transfer of vanadium ions will inevitably lead on the long term to some capacity fade as cycling proceeding, as shown in **Figure 11**. However, compared with Nafion 115, CMPSF-0.9 shows a much better capacity retention due to its much higher selectivity on vanadium ions.

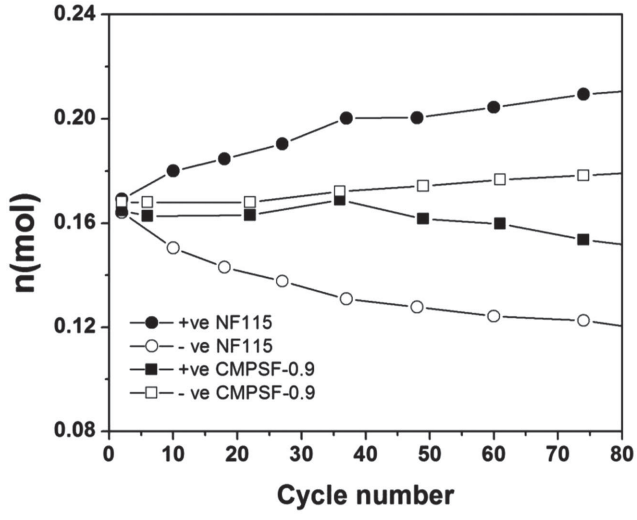

Figure 10. Molar quantity of total vanadium ions in the positive and negative half-cells.

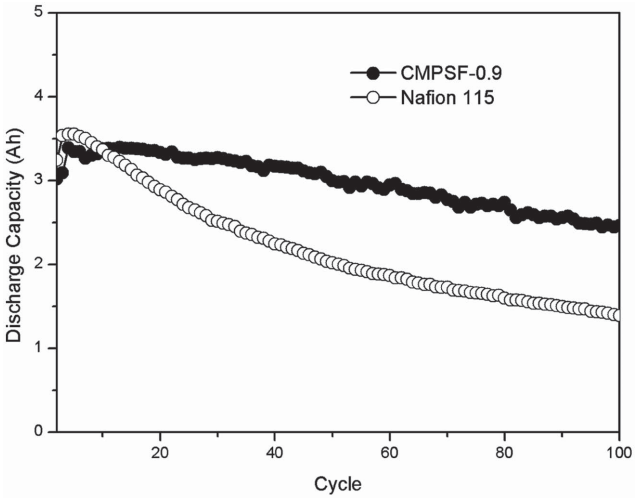

Figure 11. Discharge capacity versus cycle number of CMPSF-0.9 and Nafion 115.

3. Conclusions

In-AEMs were designed and successfully fabricated for the application of VFB. The In-AEMs membrane features a well connected internal cross linking structure, which is responsible for low vanadium permeability and excellent chemical stability. The introduction of positively charged pyridine groups can effectively restrict the vanadium transport across the membrane and improve the ionic conductivity. As a result, the VFB assembled with the optimized CMPSF membrane showed a CE of 99.2% and an EE of 81.8% at a current density of 140 mA cm^{-2}. Moreover, the In-AEM membranes exhibit excellent stability under VFB operating conditions. This work could thus provide a strategy toward the design and fabrication of high performance AEMs.

4. Experimental Section

Chloromethylation of PSF: The CMPSF polymer was prepared via a typical chloromethylation method.[6] PSF (10 g) was dissolved in chloroform (400 mL) in a three-necked round-bottomed flask. Anhydrous $SnCl_4$ (800 µL) was added into the polymer solution under nitrogen atmosphere, followed by stirring at room temperature. 99% chloromethyl methyl ether (17 mL) was then added slowly and the mixture was stirred at 55 °C for 24 h. The obtained mixture was precipitated in large amounts of rigorously stirred methanol. After stirring for 12 h, the mixture was several times filtered and washed with methanol. The obtained CMPSF was dried in vacuum at 50 °C for 24 h. The degree of chloromethylation obtained by ^{1}H NMR was about 1.30 (Supporting Information Figure S2).[17]

Membrane Preparation: CMPSF (1 g) was dissolved in *N*,*N*-dimethylacetamide (4.7 g) to form a transparent solution, after which a certain amount of 4,4′-bipyridine was added. The mixture was stirred for 7 h and then left unstirred for 3 h to remove the bubbles from the solution. The solution was cast on a clean glass plate and thermally treated at 50 °C for 12 h to obtain membranes. (denoted as CMSPF-*x*, where *x* is the ratio of 4,4′-bipyridine to chloromethyl groups of CMPSF). The thickness of the prepared membranes was 40 ± 5 µm.

TEM: Morphologies of charged bipyridine domains of fractured membrane samples were recorded by TEM (JEM-2000EX, JEOL). The

prepared membranes were treated with 0.02 M palladium chloride solution and fixed in epoxy, before being cut into thin slice samples.

Attenuated Total Reflection FTIR Spectroscopy: The chemical structures of the membranes were characterized by JASCO FTIR 4100 spectrometer. Each spectrum was recorded at the average rate of 48 scans with a resolution of 4 cm^{-1}, collected from 400 to 4000 cm^{-1} in reflection mode.

Water Uptake and Swelling: Water uptake and swelling were measured by immersing the membranes into water at room temperature for 48 h. The membranes were then taken out, wiped with a tissue paper, and quickly weighed. The water uptake was calculated as

$$\text{Water uptake}\,(\text{wt}\%) = \frac{w_{\text{wet}} - w_{\text{dry}}}{w_{\text{dry}}} \times 100\% \quad (1)$$

where w_{dry} and w_{wet} are the weights of dry and hydrated membranes, respectively. The swelling ratio was calculated by

$$\text{Swelling ratio}\,(\%) = \frac{l_{\text{wet}} - l_{\text{dry}}}{l_{\text{dry}}} \times 100\% \quad (2)$$

where l_{wet} and l_{dry} are the length of the membranes under wet and dry state, respectively.

IEC: The IEC of the membranes was determined by a titration method.[2n] The membrane was initially immersed in 1 M $NaNO_3$ solution for 24 h to convert the ion exchange groups into Cl^-. The solution was then titrated with 0.1 M $AgNO_3$ by using K_2CrO_4 as colorimetric indicator. The IEC was calculated via

$$\text{IEC} = \frac{\Delta V_{\text{AgNO3}} C_{\text{AgNO3}}}{m_{\text{d}}} \quad (3)$$

where m_d is the mass of the dry membrane, ΔV_{AgNO3} is the consumed volume of $AgNO_3$ solution, and C_{AgNO3} is the concentration of $AgNO_3$ solution.

Vanadium Permeability: Vanadium permeability across the membrane was measured by using a diffusion cell as follows. A membrane was assembled between two compartments. The left compartment was filled with a 1.5 M $VOSO_4$ in 3 M H_2SO_4 solution, and the right one with a 1.5 M $MgSO_4$ in 3 M H_2SO_4 solution. Both chambers were vigorously stirred to minimize concentration polarization. Samples from the right compartment were taken at a regular time interval. The concentration of VO^{2+} was measured by using a UV–vis spectrometer (JASCO, FTIR 4100, Japan).

Area Resistance: The area resistance of a membrane was measured via a conductivity cell. The cell was filled with 0.5 M H_2SO_4 in each compartment separated by a membrane with an effective area of 1 cm^2. The electric resistance was measured by using an electrochemical impedance spectroscopy (EIS) over a frequency range from 1 kHz to 1 MHz. The area resistance was calculated by the following equation:

$$r = (r_2 - r_1) \times s \quad (4)$$

where r_1 and r_2 are the electric resistances of the cell without and with a membrane, respectively, and s was the effective area of the membrane.

Ion Conductivity: A conductivity cell was utilized to measure the ion conductivity of the membrane. The membranes were immersed into 0.5 M NaCl for 24 h before measurement. The cell was assembled with a membrane and filled with 0.5 M NaCl. The effective area of membrane is 1 cm × 1 cm. The electric resistance was measured by using EIS. The ion conductivity of the membranes was calculated using following equation:

$$\sigma = \frac{L}{RA} w \quad (5)$$

where σ is the ion conductivity (S cm^{-1}), L is the thickness of the membranes (cm), A is the effective area of the membrane (cm^2), and R is the membrane resistance (Ω).

VFB Single Cell Performance: A VFB single cell was assembled by sandwiching a membrane with two carbon felt electrodes, clamped by two polar plates. All these components were fixed between two stainless plates. The effective area of the membrane was 3 × 3 cm^2. A 30 mL 1.5 M V^{2+}/V^{3+} in 3.0 M H_2SO_4 solutions and 1.5 M VO^{2+}/VO_2^+ in 3.0 M H_2SO_4 solutions were served as negative and positive electrolytes, respectively, and cyclically pumped into the corresponding half-cell. The battery performance test was conducted by Arbin BT 2000 at a constant current density ranging from 80 to 140 mA cm^{-2}. The battery was charged to an upper limit voltage of 1.65 V and discharge to a lower voltage of 0.8 V, respectively, to minimize the corrosion of carbon felt electrodes and graphite polar plates. The vanadium and water transfer behavior was investigated during the cycling test. The volume of negative and positive electrolytes was 100 mL. The battery was assembled with a membrane with the effective area of 48 cm^2 and cycled at a current density of 140 mA cm^{-2}. The volume change of positive and negative half-cells was measured after discharge of each cycle. The vanadium concentration of positive and negative electrolytes was detected using a potentiometric titration.

Stability Test: To investigate the chemical stability of CMPSF membrane under the strong acidic and oxidizing condition, the VFB assembled with CMPSF-0.9 was cycled at a current density of 140 mA cm^{-2}. The ex situ stability test was carried out by immersing several pieces of 3 cm × 3 cm CMPSF membranes in 1.5 M VO_2^+ for different times at 40 °C.

Supporting Information

Supporting Information is available from the Wiley Online Library or from the author.

Acknowledgements

W.X. and Y.Z. contributed equally to this work. The authors greatly acknowledge the financial support from China Natural Science Foundation (Grant Nos. 21206158 and 21476224) and the Outstanding Young Scientist Foundation, Chinese Academy of Sciences (CAS), Dalian Municipal Outstanding Young Talent Foundation (2014J11JH131), Collaborative Innovation Center of Chemistry for Energy Materials (*i*ChEM), and KU Leuven for support in the frame of IDO 12/006 and OT (11/061), and the Flemish Government for the Methusalem Assembly of Single Active Sites (CASAS) and the Federal Government for an Interuniversity Attraction Poles (IAP) grant (FS2).

Received: January 23, 2015
Revised: February 16, 2015
Published online: March 19, 2015

[1] X. Li, H. Zhang, Z. Mai, H. Zhang, I. Vankelecom, *Energy Environ. Sci.* **2011**, *4*, 1147.

[2] a) H. Ghassemi, J. E. McGrath, *Polymer* **2004**, *45*, 5847; b) B. Gupta, A. Chapiro, *Eur. Polym. J.* **1989**, *25*, 1137; c) G.-J. Hwang, H. Ohya, *J. Membr. Sci.* **1997**, *132*, 55; d) J. Kerres, A. Ullrich, M. Hein, *J. Polym. Sci., Part A: Polym. Chem.* **2001**, *39*, 2874; e) X. Li, Y. Yu, Y. Meng, *ACS Appl. Mater. Interfaces* **2013**, *5*, 1414; f) N. T. Rebeck, Y. Li, D. M. Knauss, *J. Polym. Sci., Part B: Polym. Phys.* **2013**, *51*, 1770; g) T. Sata, M. Tsujimoto, T. Yamaguchi, K. Matsusaki, *J. Membr. Sci.* **1996**, *112*, 161; h) G. Wang, Y. Weng, J. Zhao, D. Chu, D. Xie, R. Chen, *Polym. Adv. Technol.* **2010**, *21*, 554; i) W. Wang, S. Wang, W. Li, X. Xie, *Int. J. Hydrogen Energy* **2013**, *38*, 11045; j) P. Xing, G. P. Robertson, M. D. Guiver, S. D. Mikhailenko, S. Kaliaguine, *Macromolecules* **2004**, *37*, 7960; k) X. Yan, S. Gu, G. He, X. Wu, J. Benziger, *J. Power Sources* **2014**, *250*, 90; l) X. Yan, S. Gu, G. He, X. Wu, W. Zheng, X. Ruan, *J. Membr. Sci.* **2014**, *466*,

220; m) Q. Zhang, Q. Zhang, J. Wang, S. Zhang, S. Li, *Polymer* **2010**, *51*, 5407; n) S. Zhang, C. Yin, D. Xing, D. Yang, X. Jian, *J. Membr. Sci.* **2010**, *363*, 243.

[3] W. Wang, Q. Luo, B. Li, X. Wei, L. Li, Z. Yang, *Adv. Funct. Mater.* **2013**, *23*, 970.

[4] a) C. G. Arges, V. Ramani, *Proc. Natl. Acad. Sci. U.S.A.* **2013**, *110*, 2490; b) B. Li, Q. Luo, X. Wei, Z. Nie, E. Thomsen, B. Chen, V. Sprenkle, W. Wang, *ChemSusChem* **2014**, *7*, 577; c) V. Neagu, I. Bunia, *Polym. Degrad. Stab.* **2004**, *83*, 133; d) A. A. Zagorodni, D. L. Kotova, V. F. Selemenev, *React. Funct. Polym.* **2002**, *53*, 157.

[5] a) N. Li, M. D. Guiver, *Macromolecules* **2014**, *47*, 2175; b) J. R. Varcoe, P. Atanassov, D. Dekel, A. Herring, M. Hickner, P. A. Kohl, A. Kucernak, W. Mustain, K. Nijmeijer, K. Scott, *Energy Environ. Sci.* **2014**, *7*, 3135.

[6] F. Zhang, H. Zhang, C. Qu, *ChemSusChem* **2013**, *6*, 2290.

[7] a) D. J. Bradley, P. Kjellbom, C. J. Lamb, *Cell* **1992**, *70*, 21; b) Q. Li, C. Pan, J. O. Jensen, P. Noyé, N. J. Bjerrum, *Chem. Mater.* **2007**, *19*, 350.

[8] J. Miyake, K. Fukasawa, M. Watanabe, K. Miyatake, *J. Polym. Sci., Part A: Polym. Chem.* **2014**, *52*, 383.

[9] a) B. Tian, C. W. Yan, F. H. Wang, *J. Membr. Sci.* **2004**, *234*, 51; b) J. Xi, Z. Wu, X. Teng, Y. Zhao, L. Chen, X. Qiu, *J. Mater. Chem.* **2008**, *18*, 1232; c) B. Schwenzer, J. Zhang, S. Kim, L. Li, J. Liu, Z. Yang, *ChemSusChem* **2011**, *4*, 1388.

[10] A. E. Childress, M. Elimelech, *Environ. Sci. Technol.* **2000**, *34*, 3710.

[11] S. Yun, J. Parrondo, V. Ramani, *J. Mater. Chem. A* **2014**, *2*, 6605.

[12] a) A. I. Popov, J. C. Marshall, F. B. Stute, W. B. Person, *J. Am. Chem. Soc.* **1961**, *83*, 3586; b) J. Metz, O. Schneider, M. Hanack, *Spectrochim. Acta Part A* **1982**, *38*, 1265; c) S. Sen, S. Mitra, P. Kundu, M. K. Saha, C. Krüger, J. Bruckmann, *Polyhedron* **1997**, *16*, 2475.

[13] Z. Mai, H. Zhang, H. Zhang, W. Xu, W. Wei, H. Na, X. Li, *ChemSus Chem* **2013**, *6*, 328.

[14] W. Wei, H. Zhang, X. Li, Z. Mai, H. Zhang, *J. Power Sources* **2012**, *208*, 421.

[15] a) D. Chen, M. A. Hickner, *Phys. Chem. Chem. Phys.* **2013**, *15*, 11299; b) Y. Zhizhang, L. Xianfeng, H. Jinbo, X. Wanxing, C. Jingyu, Z. Huamin, *Phys. Chem. Chem. Phys.* **2014**, *16*, 19841.

[16] Q. Luo, L. Li, W. Wang, Z. Nie, X. Wei, B. Li, B. Chen, Z. Yang, V. Sprenkle, *ChemSusChem* **2013**, *6*, 268.

[17] F. Zhang, H. Zhang, C. Qu, *J. Mater. Chem.* **2011**, *21*, 12744.